metals

MDPI

Article

Peculiarities of High-Energy Induction Heating during Surface Hardening in Hybrid Processing Conditions

Vadim Y. Skeeba [1,*], Vladimir V. Ivancivsky [1] and Nikita V. Martyushev [2]

[1] Department of Industrial Machinery Design, Novosibirsk State Technical University, 20, K. Marksa Ave., 630073 Novosibirsk, Russia; ivancivskij@corp.nstu.ru
[2] Department of Materials Science, Tomsk Polytechnic University, 30, Lenina Ave., 634050 Tomsk, Russia; martjushev@tpu.ru
* Correspondence: skeeba_vadim@mail.ru; Tel.: +7-(383)-346-17-75

Abstract: This paper presents the results obtained when combining mechanical and surface-thermal operations, using the same process equipment. The paper also demonstrates the possibility of implementing high-energy heating with high-frequency currents, and proposes using an integral temperature–time characteristic as the main parameter to specify surface quenching modes. The numerical values of the integral temperature–time characteristic are to be related to the processing modes and the depth of hardening. The experiments confirmed that an increase in the capacity will be commensurate with an increase in power consumption when a volumetric heating scheme (with a hardening depth of 0.5 mm) is realized. However, during the realization of a volumetric heating scheme, when the 0.7 mm depth of the hardened layer is at the boundary of the "hot" depth of the current penetration into the metal (the beginning of the intermediate heating scheme), the increase in the processing capacity will be higher than that in power consumption.

Keywords: heat treatment; surface hardening; high-energy heating; high-frequency currents; hybrid equipment; metals; microstructure

Citation: Skeeba, V.Y.; Ivancivsky, V.V.; Martyushev, N.V. Peculiarities of High-Energy Induction Heating during Surface Hardening in Hybrid Processing Conditions. *Metals* **2021**, *11*, 1354. https://doi.org/10.3390/met11091354

Academic Editors: Anders E. W. Jarfors and Massimo Pellizzari

Received: 30 June 2021
Accepted: 24 August 2021
Published: 28 August 2021

1. Introduction

The main aim of modern mechanical engineering development is to ensure the production of competitive and high-quality products [1–11]. In this regard, the manufacturing industry is particularly interested in the development of a new type of technological equipment that allows the implementation of methods for modifying the surface layers of parts by processing them with concentrated power sources [12–16]. Local and ultra-high-speed thermal effects allow for the obtaining of higher values of hardness, strength, and viscosity, due to the formation of a highly dispersed metastable structure on the surface of the parts with a much higher dislocation density compared to volumetric machining and traditional approaches to surface hardening [5,7–12]. The development of high-frequency heating technology related to the use of radio frequencies, as well as to the miniaturization of inductors and equipping them with ferrite cores, has led to the emergence of a new method, i.e., high-energy heating with high-frequency currents (HEH HFC). This method allows for a technological quenching process with a specific heating capacity of about 400 MW/m^2, which can successfully compete with other concentrated sources (laser, electron beam) meant for hardening the material without melting it (Figure 1) [7,12].

It is noteworthy that the preservation of constant small gaps δ (0.1–0.4 mm) between the inductor and the processed part is a necessary condition for realizing HEH HFC, which in turn tightens the requirements for quenching installations, turning them in essence into metalworking machines. Since the development of new machine tools requires a large amount of financial and labor resources, we propose the modernization of standard metal-cutting machines by equipping them with an additional concentrated power source, which can be used as a HFC generator. Taking into account the current level of microprocessor

technology development of high-frequency industrial thyristor installations, as well as the criteria for their efficient integration into a standard machine tool system, our area of interest includes high-frequency microwave generators. The combination of the two processing technologies, namely mechanical and surface-thermal operations, will allow for the elimination of the disadvantages of the monotechnologies and for the obtaining of new effects that are otherwise unattainable. The use of these types of machine tools, combined with the developed technological recommendations, can enable a multiple increase in the technical and economic efficiency of production, as well as resource and power saving. This in turn contributes to improving the competitiveness of products and to updating their technological structures [1–7,15–25]. In view of the fact that the issues of developing new hybrid machine tool systems are related to critical production and industrial technologies, in the literature there is a lack of experimental works aimed at the analysis of the efficiency of these systems' designs and introductions.

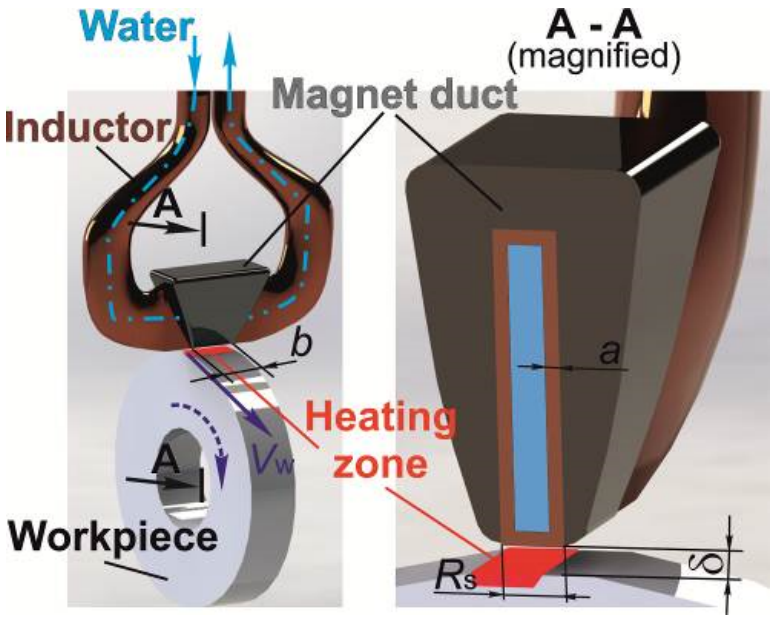

Figure 1. The scheme of HEH HFC processing.

This paper studies high-energy heating with high-frequency currents that is realized with a minimum thickness of the inductor active wire, an inductor wall thickness of a = 0.12 mm and a clearance of about 0.1 mm (Figure 1). This allows for heating by an order of magnitude greater than the previously studied modes; owing to this fact, the results presented in this paper are novel.

2. Materials and Methods

When conducting natural experiments, cylindrical parts with a diameter of d = 32 mm and a height of b = 20 mm, made of steel of 45, 60 and U8 grades, were used. The composition of the original material was determined using the optical emission spectrometer "ARL 3460" (Erich Wiesmüller, Korneuburg, Austria). The detection limit by the control elements in steel was no more than 0.01%. The relative mean square deviation of the random component of the error, when measuring the mass fractions of control elements in steel (with n = 10), was no more than 2.5%. The experimental results are presented in Tables 1–3.

Table 1. The chemical compositions of steel 45.

Elements	C	Si	Mn	S	P	Cr	Ni	Cu
Weight, (%)	0.44	0.23	0.61	0.013	0.019	0.11	0.15	0.17

Table 2. The chemical compositions of steel 60.

Elements	C	Si	Mn	S	P	Cr	Ni	Cu
Weight, (%)	0.59	0.25	0.65	0.017	0.021	0.13	0.16	0.18

Table 3. The chemical compositions of steel U8.

Elements	C	Si	Mn	S	P	Cr	Ni	Cu
Weight, (%)	0.80	0.24	0.21	0.017	0.022	0.11	0.15	0.18

To integrate the processes of mechanical and surface thermal treatment, the thread-cutting lathe of the "UT16PM" (Ulyanovsk Machine-Building Plant, Ulyanovsk, Russia) model was modernized. This modernization consisted of equipping the machine-tool system with a supplementary concentrated power source. A remote hardening scheme, implementing high-energy heating with high-frequency currents (HEHHFC), was used as a concentrated power source. A thyristor-type generator "SVCH-10" (UralInduktor, Miass, Russia) with a current operating frequency of $\omega = 400 \times 10^3$ Hz was used as a power source.

During surface quenching, a serpentine inductor (NSTU, Novosibirsk, Russia), equipped with ferrite of the N87 grade with a magnetic permeability of $\mu_i = 2200$, was used (Figure 1). The heating was carried out according to the deep-laid scheme by the continuous-sequential technique. In this case, the thickness of the strengthened layer did not exceed the depth of penetration of the current into the hot metal equal to 0.6 . . . 0.8 mm. The processing modes were as follows: specific power of the source—$q_s = (1.5–4.0) \times 10^8$ W/m^2; the travel rate of the part under the inductor was $V_w = (0.05–0.1)$ m/s. The width of the active inductor wire was $R_s = 1.2$ mm. The processing was carried out with a clearance of $\delta = 0.1–0.2$ mm. Intensive water (shower) cooling of the surface was used.

The structure was studied using the optical microscope "Carl Zeiss Axio Observer Z1m" (ZEISS, Köln, Germany). To identify the microstructure of the samples, etching with a 5%-alcoholic solution of nitric acid and a saturated solution of picric acid in the ethyl alcohol, supplemented with surface-active substances, was carried out [12]. The "Wolpert Group 402MVD" device (Yumpu, Diepoldsau, Switzerland) was used to assess the microhardness of the hardened surface layer of the part. The measurement accuracy corresponded to standards EN-ISO 6507, ASTM E384, E92 and JIS. The digital encoder resolution was 0.1 μm.

The behavior of the phase transformations, the resulting structure and the depth of quenching, including the grain size of austenite, depend on the integral temperature–time heating effect on the steel structure and are therefore determined by the shape of the thermal curve [5,7,12]. Due to the difficulty of controlling the temperatures and heating rates to specify the hardening modes of using concentrated power sources, mathematical simulation of the processes occurring in the material surface layers during surface quenching has become widespread [5,12].

The average speed and the maximum heating temperature, as the main parameters for the surface quenching modes, are not accurate enough to characterize the temperature and time conditions of phase transformations during steel austenitization. In addition to these parameters, it is necessary to take into account the average cooling rate and the time of the material's residence within the temperature range of phase transformations. Therefore, the processing modes should be specified in such a way as to provide the necessary thermal cycles with the specified parameters in the surface layers of the material. As shown in certain studies [5,12], it is not possible to establish an unambiguous relationship between the numerical values of these parameters with the processing modes and the quality characteristics of the hardened layer. However, it is obvious that the numerical values of the parameters of thermal cycles are determined by the amount of transmitted power and the nature of its distribution in the material.

In this regard, based on certain works [5,7,12], we propose using the integral temperature–time characteristic S, which combines all the listed parameters of thermal cycles, as the main parameter for specifying the surface quenching modes. The process of austenite formation takes place in the time period of $\tau_t = \tau_3 - \tau_1$ (Figure 2) regardless of whether the thermal curve is ascending or descending in this time period. This means that the total time τ_B and the temperatures at which the austenitization process occurs can be characterized by the area (S_{ABC}), bounded at the top by the heating curve and at the bottom by the straight line corresponding to the temperature A_{C1}:

$$S = \int_{\tau_1}^{\tau_3} T(\tau)d\tau - A_{C1}(\tau_3 - \tau_1) \quad (1)$$

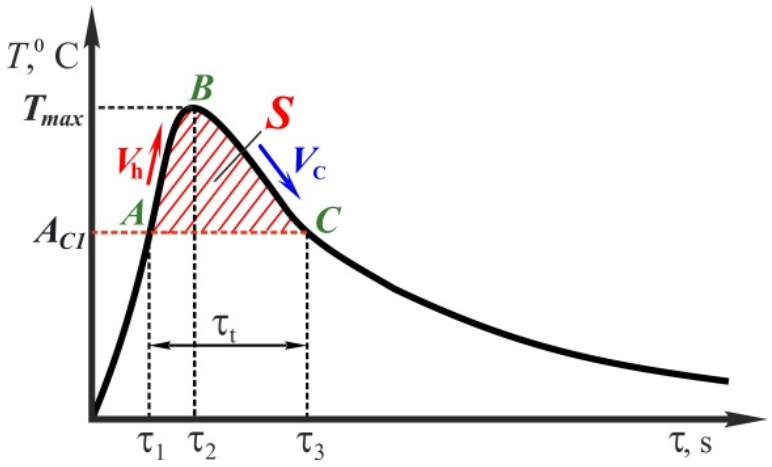

Figure 2. Kinetic curve of steel heating and cooling during quenching.

The physical meaning of this characteristic becomes clear, proceeding from:

$$S = Q \cdot R_T$$

where Q is the power, J; R_T is the thermal resistance of the material, °C·s/J.

The thermal resistance of a metal is the ability of a material to resist heat transfer. Let us consider a metal heated above the temperature A_{C1}. In this case, the numerical value of the metal's thermal resistance depends not only on the thermal conductivity coefficient, but also on the structural phase transitions that mainly occur endothermally in this temperature range, accompanied by heat absorption. In other words, this characteristic indirectly determines the amount of power transmitted to the material and spent on structural phase transformations. It can be easily calculated based on the dependence (1) during simulation of the temperature fields in the material [5,7,12].

Based on the above-mentioned, in order to develop a method for specifying surface quenching modes in hybrid processing conditions, it is necessary to establish the relationship between the numerical values of the integral temperature–time characteristic and the processing modes on the one hand, and the hardening depth on the other. This problem is solved by concurrent simulation of temperature fields and structural phase transformations in the material [12].

By means of the finite-element simulation of temperature fields in the material, during high-energy heating with high-frequency currents, parameters of thermal cycles (heating rate, maximum heating temperature, cooling rate and the time of the material's residence above the point A_{C1}) were obtained in each surface layer under study depending on processing modes (rate and specific power). Then, the process of steel austenization was simulated. Based on these data, the decay of the resulted austenite was analyzed at the cooling stage. It is sufficient to use thermal-kinetic austenite decay curves for the

appropriate steel grade in the material layers where complete austenite homogenization takes place. In this case, having values of cooling rates in the temperature range of the least stability of austenite and in the temperature range of martensite formation, i.e., having a cooling curve, it is possible to forecast the percentage of the composition of structures formed during austenite decay, and the microhardness level typical of this composition of structures. At the same time, it is necessary to note that the highly dispersed structure of martensite is to be obtained in cases when austenite homogenization finishes at the same moment the material leaves the phase transition temperature band.

The finite element model was constructed using the software packages ANSYS and SYSWELD, using numerical methods for solving differential equations of transient heat conduction (Fourier equation), carbon diffusion (Fick's 2nd law) and elastoplastic behavior of the material.

The finite element model was prepared in the ANSYS software (version 19.1, Canonsburg, PA, USA) package. The ANSYS Meshing generator formed a hexahedral mesh using the following types of finite elements: solid bodies were simulated with 8-node SOLID 45 tetrahedra; surface bodies were modeled with 4-node 4-angle shell-type elements–SHELL 63; line bodies were simulated with 2-node linear elements LINK 8. The size of the finite elements was 0.01 … 1 mm. When creating a finite element model, the following components are created. The first component is "Volume", a group of three-dimensional elements denoting the processed object. The second component is "Trajectory", a group of one-dimensional elements that determines the motion pattern of a high-concentration energy source. The third is "Reference"—a reference equidistant—a group of one-dimensional elements that contributes to the orientation of the local coordinate system of the energy source. The fourth component is "StartElem", starting elements of the beginning of the source operation. The fifth is "StartNodes" and "EndNodes"—starting and end nodes on the motion pattern. The sixth component is "Skin", a group of two-dimensional elements denoting the surfaces along which convective and radiative heat losses occur. The last one is "ClampedNodes", a group of nodes along which the disk is fixed (Figure 3).

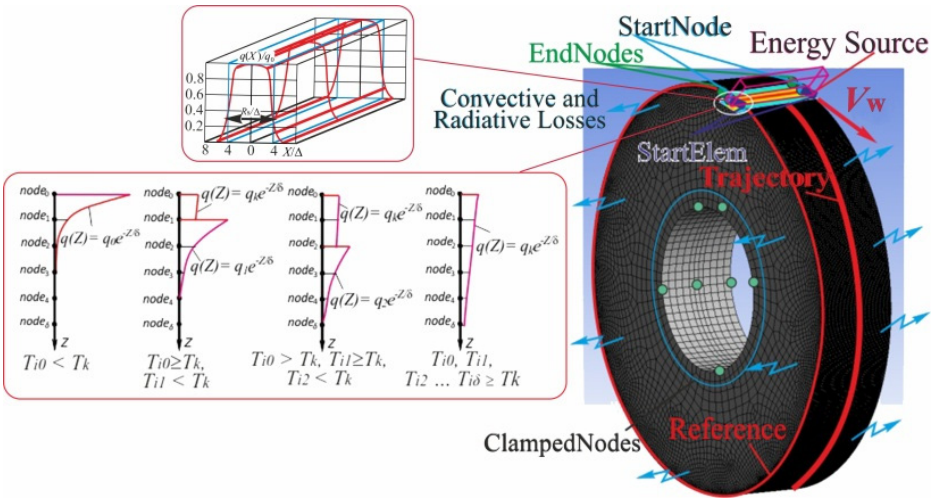

Figure 3. Finite element model of the HEH HFC process.

The process of high-energy heating by high-frequency currents was simulated in the SYSWELD software (version 2010, Rungis, France) package, which allows for the use of a model of the elastic-viscoplastic behavior of the material and the modern mathematical apparatus, the calculation of temperature fields, and the distribution of structural components, internal stresses and deformations. During the preparation of the finite element model, the specific character of the distribution of the specific power of the HFC heating source directly under the inductor and throughout the depth of the material was taken into account [7,12].

3. Results and Discussion

Based on the results presented in Figure 4, the required minimum values of the characteristic S, appropriate for the production of a hardened layer, vary within ($4.3 > S > 2.5$) °C·s. The dependence data (Figure 4) were obtained as a result of the concurrent simulation of temperature fields and structural phase changes in the material. Further, line 2 represents a minimal value of the characteristic S for obtaining 50% of martensite after cooling. However, as the numerical and field experiments show, in most cases, the maximum values of the characteristic exceed the above-mentioned values.

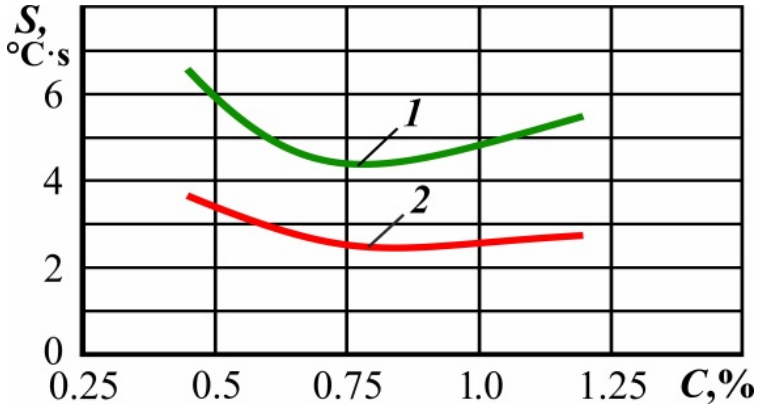

Figure 4. Dependence of the temperature–time characteristic on the carbon concentration in steel: (1) obtaining homogeneous austenite; (2) carbon content in austenite, with which 50% of martensite can be fixed at the cooling stage.

This happens because the distribution of the characteristic S values throughout the depth of the material is primarily not uniform. The lower the depth of the hardened layer, the closer the S characteristic values are to the recommended values, which additionally confirms the greater efficiency of the deep heating scheme in relation to the surface one.

The maximum values of the characteristic S when realizing the deep heating scheme are at 6.2 °C·s, and those of the surface heating scheme are at 500 °C·s. Therefore, in the surface heating scheme, the surface layers of the material are subject to an excess amount of power in relation to the value required for the austenite homogenization. This eventually leads to the growth of the austenitic grain, and hence to the formation of a larger martensite structure during cooling.

The regularity of the changes to the value of the characteristic S corresponds to the nature of the changes to the values of the maximum temperatures at the depth of the material. The maximum values of this characteristic for these power sources are reached at a depth of about 0.2 mm. Based on this, it is possible to establish the dependence of the characteristic S value at the depth of 0.2 mm on the value of the resulting hardened layer.

The surface quenching of steels 45, 60 and U8 by HEH HFC is presented by the following dependence:

$$S(h) = 0.55 + 3.69h - 5.95h^2 + 38.62h^3 \quad (2)$$

$$S(h) = 0.77 + 3.33h - 5.36h^2 + 45.17h^3 \quad (3)$$

$$S(h) = 0.90 + 3.19h - 5.14h^2 + 50.18h^3 \quad (4)$$

To establish the functional dependence of the integral temperature–time characteristic S on the technological processing modes, the experimental data were processed using the software products *STATISTICA 6.0* (StatSoft, Tulsa, OK, USA) and *Table Curve 3D v 4.0* (Merck, Darmstadt, Germany). The maximum error did not exceed 5%. In this case, the specific power and the travel rate of the heating source are taken as variable values. This depends primarily on the fact that the changes to the size of the HEH HFC source are

associated with the time-consuming manufacture of a new inductor. Therefore, in case of induction heating, it is customary to initially set the size of the source, and then to select two other technological parameters.

Figure 5 shows the results of these studies through the examples of the surface quenching of steels U8 and 45 using HEH HFC.

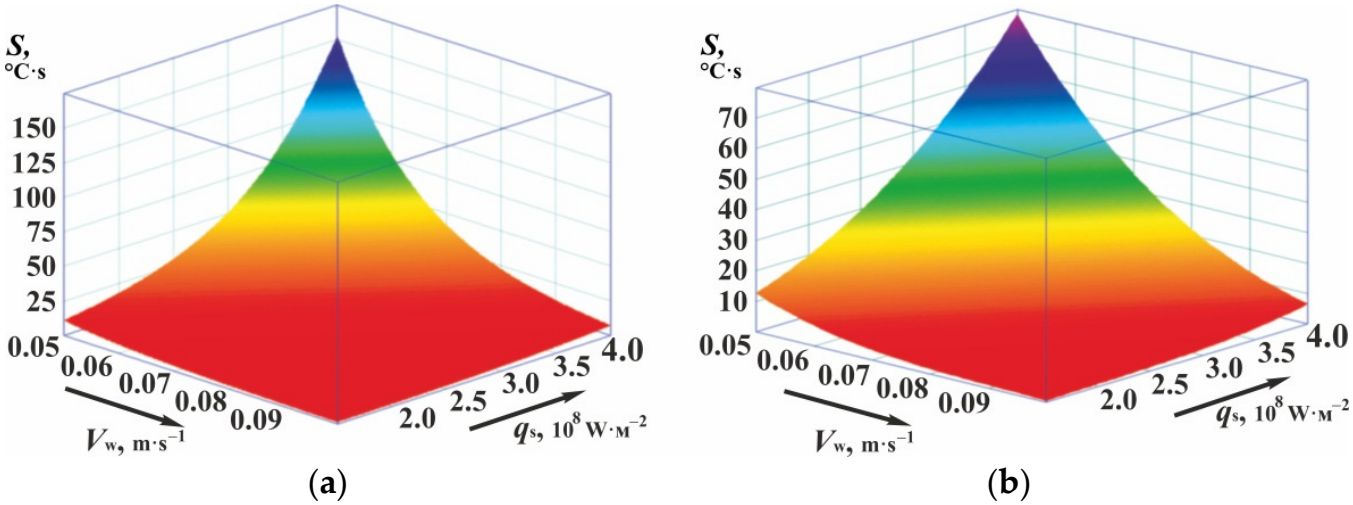

Figure 5. Functional dependencies of $S(q_s,V_w)$: (**a**) for steel U8; (**b**) for steel 45.

In this way, there is the established dependence of the characteristic S on the depth of hardening on the one hand, and on the processing modes on the other. This allows for the specification of rational modes of the surface hardening of steel parts, for example, operating purely in conditions of wear. For these types of parts, the hardness and depth of the hardened layer are the main technological parameters. The desired hardness of the hardened layer is obtained by selecting the appropriate grade of steel, while the required depth of hardening is provided using appropriate technological modes [5,7,12].

Let us consider the proposed method for specifying surface quenching modes providing only the depth of the quenched layer in the following example.

It is required to harden a cylindrical disc-type part (Figure 1) made of the 45-grade steel and the U8 steel by applying HEH HFC. Its height is b = 20 mm, diameter (d) = 32 mm (respectively, its circumference is $l \approx 100$ mm), with a width of the active inductor wire of R_s = 2 mm to a depth of h_1 = 0.5 mm and h_2 = 0.7 mm.

According to the depth of the hardened layer (h), specified in the drawing and based on the dependencies (2) and (4), we obtain the values of the integral temperature–time characteristic S. This characteristic must be achieved at a depth of 0.2 mm, equal, respectively, for steel U8 with h_1—5.74 °C·s and h_2—13.46 °C·s; for steel 45 with h_1—7.485 °C·s and h_2—17.83 °C·s. Further, based on these values of the characteristic S, according to the functional dependencies (Figure 5a,b), we obtain the functional dependence of technological modes V_w and q_s. Figure 6 shows the surface sections for steel 45 (see Figure 5b) and steel U8 (see Figure 5a) with the appropriate values of the characteristic S. Any combination of modes (V_w and q_s) that corresponds to these dependencies allows for the achievement of the target value of the integral characteristic at the depth of 0.2 mm, and therefore provides the specified depth of hardening under appropriate cooling conditions.

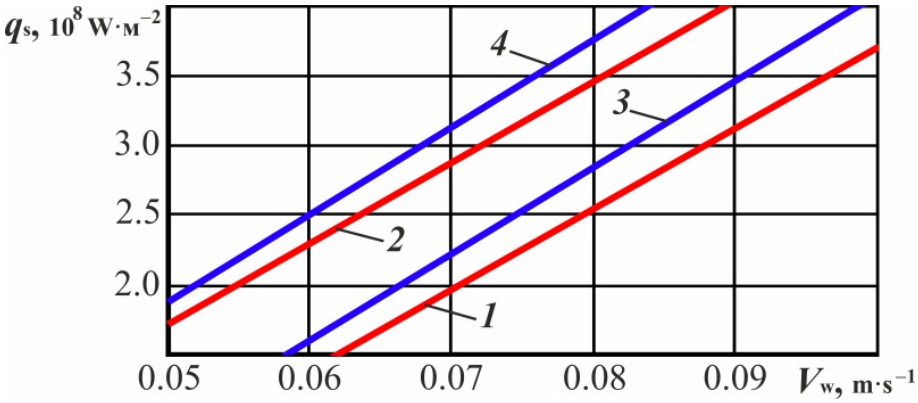

Figure 6. The dependence of the source specific power on its travel rate when quenching steel U8 and steel 45 by HEH HGC to a depth of: 0.5 mm for steel U8 (1) and steel 45 (3); 0.7 mm for steel U8 (2) and steel 45 (4).

The proposed method for specifying surface hardening modes in hybrid processing conditions was tested based on real samples. Figure 7 presents the results of the optical microscopy and microhardness measurement data. Analyzing the distribution graphs of the surface layer microhardness, one can specify three typical zones (Figure 7a,b). Zone I is characterized by a stable average value of the microhardness level. Zone II is a transitional area. Zone III is an area that is not subject to structural and phase changes. Let the depth of the hardened layer be the distance from the surface to the zone with a structure containing 50% of martensite. In its turn, the transition layer is a zone between the surface layer of the hardened steel with a stable average level of microhardness and a zone of the material where no structural phase changes have occurred. It is theoretically proven and experimentally confirmed that the established relationship between the integral temperature–time characteristic and the depth of hardening on the one hand, and the processing modes on the other, provides the required depth and hardness of the hardened layer. In this case, it becomes possible to guarantee the required relative size of the transition layer, which creates conditions for a rational distribution of residual stresses over the depth of hardening.

Owing to the fact that the efficiency of any processing is evaluated according to the criteria of increasing the capacity and reducing power consumption, we compared these characteristics within the resulting range of modes. The processing capacity (technological performance—*TP*) is calculated according to the actual (machining) time (τ_m):

$$TP_m = 1/\tau_m = V_w/l$$

Therefore, it increases in direct proportion to the travel rate of the heating source.

The processing power consumption (E) is evaluated according to the following dependence:

$$E = \frac{q_s b R_s}{\frac{V_w}{l}} = \frac{q_s b R_s l}{V_w}$$

The results of power consumption calculations for the range of modes appropriate for curves 1–4 (Figure 6) are shown in Figure 8.

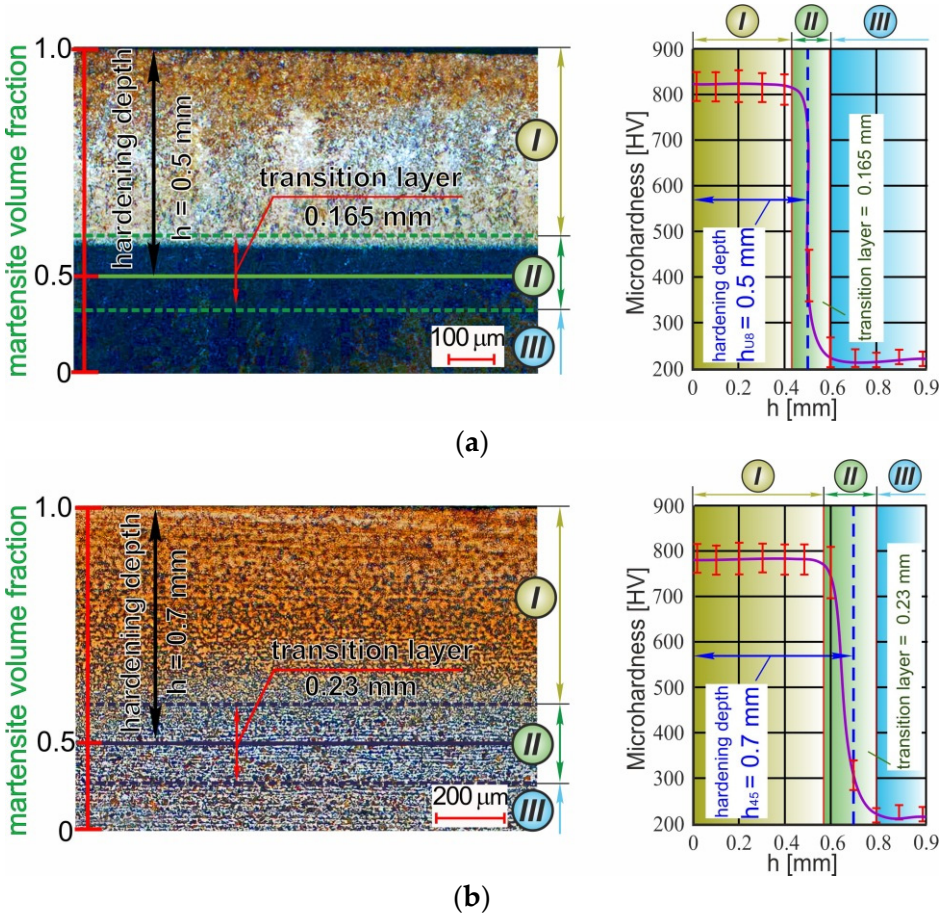

Figure 7. Microstructure of the hardened layer: (**a**) carbon tool steel (0.8% C), depth of the hardened layer: 0.5 mm; (**b**) carbon constructional steel (0.45% C), depth of the hardened layer: 0.7 mm.

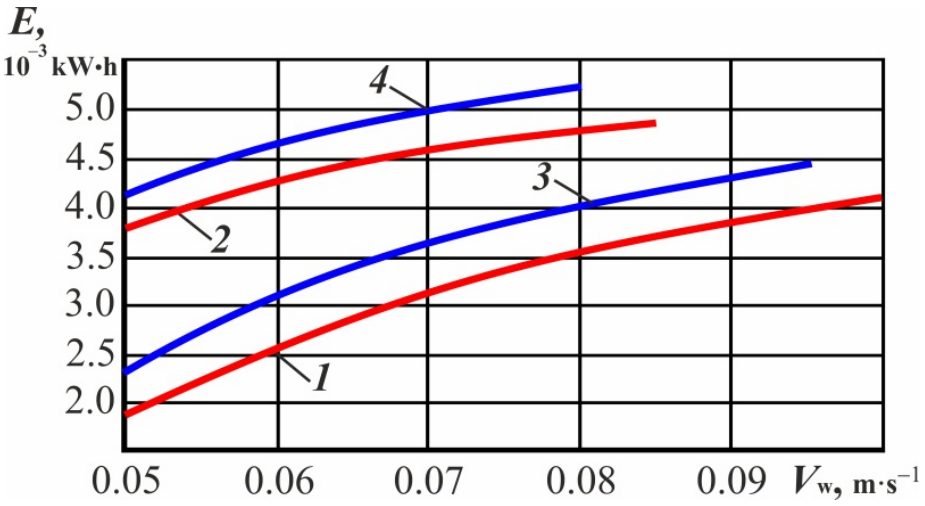

Figure 8. The dependence of power consumption on the travel rate of the heating source when quenching steel U8 and steel 45 using HEH HFC to a depth of 0.5 mm for steel U8 (1) and steel 45 (3); to a depth of 0.7 mm for steel U8 (2) and for steel 45 (4).

The results of the numerical simulation showed (Figure 8) that the increase in the capacity was accompanied by a corresponding increase in processing power consumption. Let us compare the minimum and maximum combinations of modes of the obtained range:

(1) when quenching the U8 steel to a depth of 0.5 mm: $TP_{m_{\min}} = 0.5\ \mathrm{s}^{-1}$, $E_{\min} = 0.0019\ \mathrm{kW \cdot h}$, $TP_{m_{\max}} = 1.0\ \mathrm{s}^{-1}$, $E_{\max} = 0.0041\ \mathrm{kW \cdot h}$, and the capacity was doubled,

while the power consumption increased 2.15 times. Consequently, the increase in power consumption was 1.075 times higher than that in the capacity;

(2) when quenching the 45-grade steel to a depth of 0.5 mm: $TP_{m_{\min}} = 0.5\ s^{-1}$, $E_{\min} = 0.00216\ kW \cdot h$, $TP_{m_{\max}} = 0.95\ s^{-1}$, $E_{\max} = 0.0044\ kW \cdot h$, the capacity increased 1.9 times, and the power consumption increased 2.04 times. Consequently, the increase in power consumption was 1.074 times higher than that in the capacity;

(3) when quenching the U8 steel to a depth of 0.7 mm: $TP_{m_{\min}} = 0.5\ s^{-1}$, $E_{\min} = 0.0038\ kW \cdot h$, $TP_{m_{\max}} = 0.85\ s^{-1}$, $E_{\max} = 0.0049\ kW \cdot h$, the capacity increased 1.7 times, and the power consumption increased 1.29 times. Consequently, the increase in power consumption was 1.32 times higher than that in the capacity;

(4) when quenching the 45-grade steel to a depth of 0.7 mm: $TP_{m_{\min}} = 0.5\ s^{-1}$, $E_{\min} = 0.004168\ kW \cdot h$, $TP_{m_{\max}} = 0.80\ s^{-1}$, $E_{\max} = 0.0052\ kW \cdot h$, the capacity increased 1.6 times, and the power consumption increased 1.25 times. Consequently, the increase in the capacity was 1.28 times higher than that in power consumption.

4. Conclusions

Analyzing the obtained results, we can draw the following conclusions:

(1) When realizing a purely volumetric heating scheme (with a hardening depth of 0.5 mm), the increase in the processing capacity will be commensurate with the increase in power consumption.

(2) When realizing a volumetric heating scheme, if the 0.7 mm depth of the hardened layer is at the boundary of the "hot" depth of the current penetration into the metal δ_K (the beginning of the intermediate heating scheme), the increase in the processing capacity will be higher than that in power consumption.

The latter can be explained by the fact that the specific heating power is higher in relation to a purely volumetric scheme, and the temperature gradient over the depth of the material is greater as well. Consequently, due to the thermal conductivity of the material, a large proportion of power is spent on heating the deeper layers of the material. An increase in the travel rate of the source decreases the share of power directed, owing to thermal conductivity, to the depth of the material, but it is still higher than that when realizing a purely volumetric heating scheme. Based on this, we assume that when realizing a surface heating scheme (the deeper layers of the material must be heated to the temperatures of phase transitions due to thermal conductivity), the increase in the processing capacity within the resulting range of modes can be accompanied by a decrease in power consumption.

Summing up the above-mentioned information, we can note that when realizing a volumetric heating scheme, along with an increase in the processing capacity, power consumption increases at almost the same intensity. When realizing the intermediate heating scheme, along with an increase in the processing capacity, power consumption decreases at the beginning of the studied range of modes, and then the power consumption increases. The surface heating scheme is peculiar because the power consumption for processing decreases along with increased productivity, although the overall level of power consumption is much higher than that of the volumetric heating scheme.

In this regard, we believe that for the parts operating in wear conditions, it is required to specify maximum surface hardening modes within the established range in accordance with the technical conditions of the heating source and process equipment.

Author Contributions: V.Y.S., V.V.I. and N.V.M. wrote the paper; V.Y.S. and V.V.I. conducted the experiment; N.V.M. carried out mathematical processing of the test results. All authors have read and agreed to the published version of the manuscript.

Funding: The research was funded by RFBR and Novosibirsk region, project number 20-48-540016.

Data Availability Statement: Not applicable.

Acknowledgments: Research were conducted at core facility "Structure, mechanical and physical properties of materials" (Novosibirsk State Technical University, Novosibirsk, Russia).

Conflicts of Interest: The authors declare no conflict of interest.

References

1. Makarov, V.M. Well integrated technological systems: Prospects and problems of implementation. *Repair. Innovation. Technol. Mod.* **2011**, *6*, 20–23.
2. Khatir, F.A.; Sadeghi, M.H.; Akar, S. Investigation of surface integrity in the laser-assisted turning of AISI 4340 hardened steel. *J. Manuf. Process.* **2021**, *61*, 173–189. [CrossRef]
3. Makarov, V.M.; Lukina, S.V. Unique synergy of hybrid machines. *Repair. Innovation Technol. Mod.* **2016**, *8*, 18–25.
4. Garro, O.; Martin, P.; Veron, M. Shiva a Multiarms Machine Tool. *CIRP Ann. Manuf. Technol.* **1993**, *42*, 433–436. [CrossRef]
5. Skeeba, V.; Pushnin, V.; Erohin, I.; Kornev, D. Integration of production steps on a single equipment. *Mater. Manuf. Process.* **2015**, *30*, 1408–1411. [CrossRef]
6. Borisov, M.A.; Lobanov, D.V.; Yanyushkin, A.S. Hybrid technology of electrochemical processing of complex profiles. *Obrab. Met.* **2019**, *21*, 25–34. [CrossRef]
7. Skeeba, V.Y.; Ivantcivsky, V.V. *Hybrid Metal Working Equipment: Improving the Effectiveness of the Details Processing under the Integration of Surface Quenching and Abrasive Grinding*; NSTU Publ.: Novosibirsk, Russia, 2018; p. 312, ISBN 978-5-7782-3690-5.
8. Mitsuishi, M.; Ueda, K.; Kimura, F. *Manufacturing Systems and Technologies for the New Frontier*; Springer Publ.: London, UK, 2008; p. 556, ISBN 978-1-84800-267-8. [CrossRef]
9. Liu, J.; Ye, C.; Dong, Y. Recent development of thermally assisted surface hardening techniques: A review. *Adv. Ind. Manuf. Eng.* **2021**, *2*, 100006. [CrossRef]
10. Lobanov, D.V.; Arkhipov, P.V.; Yanyushkin, A.S.; Skeeba, V.Y. Research of Influence Electric Conditions Combined ElectroDiamond Processing by on Specific Consumption of Wheel. *IOP Conf. Ser. Mater. Sci. Eng.* **2016**, *142*, 012081. [CrossRef]
11. Brecher, C.; Özdemir, D. *Integrative Production Technology: Theory and Applications*; Springer International Publ.: London, UK, 2017; p. 1100. Hardcover ISBN 978-3-319-47451-9; eBook ISBN 978-3-319-47452-6. [CrossRef]
12. Ivancivsky, V.V.; Skeeba, V.Y. *Hybrid Metal Working Equipment. Technological Aspects of Integrating the Operations of Surface Hardening and Abrasive Grinding*; NSTU Publ.: Novosibirsk, Russia, 2019; p. 348, ISBN 978-5-7782-3988-3.
13. Mühl, F.; Jarms, J.; Kaiser, D.; Dietrich, S.; Schulze, V. Tailored bainitic-martensitic microstructures by means of inductive surface hardening for AISI4140. *Mater. Des.* **2020**, *195*, 108964. [CrossRef]
14. Sales, W.F.; Schoop, J.; Silva, L.R.R.; Machado, Á.R.; Jawahir, I.S. A review of surface integrity in machining of hardened steels. *J. Manuf. Process.* **2020**, *58*, 136–162. [CrossRef]
15. Ding, H.T.; Shin, Y.C. Laser-assisted machining of hardened steel parts with surface integrity analysis. *Int. J. Mach. Tools Manuf.* **2010**, *50*, 106–114. [CrossRef]
16. You, K.; Yan, G.; Luo, X.; Gilchrist, M.D.; Fang, F. Advances in laser assisted machining of hard and brittle materials. *J. Manuf. Process.* **2020**, *58*, 677–692. [CrossRef]
17. Lauwers, B.; Klocke, F.; Klink, A.; Tekkaya, A.E.; Neugebauer, R.; Mcintosh, D. Hybrid processes in manufacturing. *CIRP Ann. Manuf. Technol.* **2014**, *63*, 561–583. [CrossRef]
18. Yanyushkin, A.S.; Lobanov, D.V.; Arkhipov, P.V. Research of influence of electric conditions of the combined electro-diamond machining on quality of grinding of hard alloys. *IOP Conf. Ser. Mater. Sci. Eng.* **2015**, *91*, 012051. [CrossRef]
19. Jeon, Y.; Lee, C.M. Current research trend on laser assisted machining. *Int. J. Precis. Eng. Manuf.* **2012**, *13*, 311–317. [CrossRef]
20. Berenji, K.R.; Karagüzel, U.; Özlü, E.; Budak, E. Effects of turn-milling conditions on chip formation and surface finish. *CIRP Ann. Manuf. Technol.* **2019**, *68*, 113–116. [CrossRef]
21. Moriwaki, T. Multi-functional machine tool. *CIRP Ann. Manuf. Technol.* **2008**, *57*, 736–749. [CrossRef]
22. Boivie, K.; Karlsen, R.; Ystgaard, P. The concept of hybrid manufacturing for high performance parts. *South Afr. J. Ind. Eng.* **2012**, *23*, 106–115. [CrossRef]
23. Yamazaki, T. Development of A Hybrid Multi-tasking Machine Tool: Integration of Additive Manufacturing Technology with CNC Machining. *Procedia CIRP* **2016**, *42*, 81–86. [CrossRef]
24. Yang, Y.; Gong, Y.; Qu, S.; Rong, Y.; Sun, Y.; Cai, M. Densification, surface morphology, microstructure and mechanical properties of 316L fabricated by hybrid manufacturing. *Int. J. Adv. Manuf. Technol.* **2018**, *97*, 2687–2696. [CrossRef]
25. Nagae, A. Development Trend of Multi-tasking Machines. *Proc. JSPE Semest. Meet.* **2005**, *2005S*, 430. [CrossRef]